Osteoarthritis and Cartilage 27 (2019) 1382–1391

Osteoarthritis and Cartilage

Through-thickness patterns of shear strain evolve in early osteoarthritis

F. Maier †, C.G. Lewis ‡, D.M. Pierce † § *

† University of Connecticut, Department of Mechanical Engineering, Storrs, CT, USA
‡ Hartford Healthcare, Bone & Joint Institute, Hartford, CT, USA
§ University of Connecticut, Department of Biomedical Engineering, Storrs, CT, USA

ARTICLE INFO

Article history:
Received 6 October 2018
Accepted 27 April 2019

Keywords:
Human articular cartilage
Shear strain pattern
Large strain
Zonal architecture
Early osteoarthritis

SUMMARY

Objective: Given the structural changes associated with the progression of Osteoarthritis (OA), we hypothesized that patterns of through-thickness, large-strain shear evolve with early-stage OA. We therefore aimed to determine whether and how patterns of shear strains change during early-stage OA to 1) gain insight into the progression of OA by quantifying changes in local deformations; 2) gauge the potential of patterns in shear strain to serve as image-based biomarkers of early-stage OA; and 3) provide high-resolution, through-thickness data for proposing, fitting, and validating constitutive models for cartilage.

Design: We completed displacement-driven, large-strain shear tests (5, 10, 15%) on 44 specimens of variably advanced osteoarthritic human articular cartilage as determined by both Osteoarthritis Research Society International (OARSI) grade and PLM-CO score. We recorded the through-thickness deformations with a stereo-camera system and processed these data using digital image correlation (DIC) to determine full-thickness patterns of strains and relative zonal recruitments, i.e., the average shear strain in a through-thickness zone weighted by its relative thickness and normalized by the applied strain.

Results: We observed three general shapes for the curves of averaged through-thickness, Green–Lagrange shear strains during progression of OA. We also observed that during the progression of OA only the deep zone is recruited differently under shear in a statistically significant way.

Conclusions: We propose that changes in through-thickness patterns of shear strain could provide sensitive biomarkers for early clinical detection of OA. The relative zonal recruitment of the deep zone decreases with progressing OA (OARSI grade) and microstructural remodeling (PLM-CO score), which do not consistently affect recruitment of the superficial and middle zones.

Introduction

With progression of osteoarthritis (OA), degenerated cartilage eventually becomes unable to withstand normal (daily) intra-tissue mechanical loads, thus initiating a sustained degradation of the extracellular matrix (ECM).[1,2] Although no treatment currently exists to fully restore damaged or degenerated cartilage,[3] detection/monitoring of preclinical degeneration may facilitate earlier treatments and allow for interventions before cartilage degenerates beyond repair.[4]

Image-based methods that can detect early degeneration of cartilage remain clinically untenable. Current image-based methods that can detect early-stage degeneration track the progression of OA via histology (e.g., Osteoarthritis Research Society International (OARSI) grading[5] or adapted Mankin grading[6]), but these methods require tissue explants generally unavailable in a clinical setting. Clinically feasible methods to quantify degeneration of cartilage rely on arthroscopic evaluation (e.g., Outerbridge[7]) or magnetic resonance imaging (MRI) (e.g., protocol by the International Cartilage Repair Society (ICRS)[8]), but lack the sensitivity to detect the onset of degeneration (i.e., early-stage OA).

Early minute changes in the structure of the collagen network that precede other more substantial changes (e.g., loss of proteoglycan (PG)) can alter the mechanical responses of cartilage even at the onset of OA.[9] OA-induced degeneration affects the orientations

* Address correspondence and reprint requests to: D.M. Pierce, Department of Mechanical Engineering, University of Connecticut, 191 Auditorium Road, Unit 3139, Storrs, CT 06269-3139, USA.
E-mail address: dmpierce@engr.uconn.edu (D.M. Pierce).

https://doi.org/10.1016/j.joca.2019.04.018
1063-4584/

of collagen fibers across the cartilage surface, as well as through the thickness, and typically initiates with fibrillation of the superficial zone (SZ).[10–12] Thus, intra-tissue mechanics (e.g., the through-thickness shear strain magnitude measured by displacement under applied load MRI (dualMRI)[13]) may provide more sensitive image-based (non-invasive) biomarkers for early-stage degeneration of cartilage. Such imaging methods highlight the potential for detecting the onset of OA via changes in local (intra-tissue) mechanics.

Previous studies of mechanical shear have shed significant light on structure–function relationships in cartilage.[14–18] Studies that use digital image correlation (DIC) have illuminated the intra-tissue mechanics and local mechanobiological environment within cartilage under compression[19,20] or shear.[16,18,21,17] The shear modulus varies by up to two orders of magnitude through the thickness of healthy cartilage,[16,22] and the local shear-strain patterns correspond to the underlying collagen structure during tissue maturation.[17] Further, both local and bulk shear strains increase with tissue degeneration and friction (lubricant–synovial fluid vs phosphate buffered saline (PBS)).[18] These studies do not, however, employ the large-strain kinematics and nonlinear mechanics required to capture the large deformations cartilage undergoes *in vivo* (greater than 20% compression[23,24] causing complex loadings[25,26]). Furthermore, most studies do not include both large-strain deformations and human tissues, two factors essential to understanding and modeling cartilage biomechanics *in vivo*, and no data currently exists on large-strain shear of human cartilage at progressing stages of degeneration.

Given the structural changes associated with the progression of OA, we hypothesized that patterns of through-thickness, large-strain shear evolve with early-stage OA. We therefore aimed to determine whether and how patterns of shear strains change during early-stage OA to 1) gain insight into the progression of OA by quantifying changes in local deformations, and thus the mechanobiological environment of embedded constituents; 2) gauge the potential of patterns in shear strain to serve as image-based biomarkers of early-stage OA; and 3) provide high-resolution, through-thickness data for proposing, fitting, and validating constitutive models.

Materials and methods

Using a triaxial shear testing device (Messphysik, Fuerstenfeld, AT) we completed displacement-driven, large-strain shear tests (following a protocol detailed previously[27]) on 44 specimens of progressively more severely osteoarthritic (according to both OARSI grade[5] and Polarized Light Microscopy Collagen Orientation (PLM-CO) score[12]) human articular cartilage. We recorded through-thickness deformations with a stereo-camera system and processed these data using DIC to determine full-thickness patterns of shear strains and relative zonal recruitments, i.e., the average shear strain in a through-thickness zone weighted by its relative thickness and normalized by the applied strain.

Preparation of specimens

We harvested nine lateral femoral condyles ($n = 9$, two male and seven female, 67.0±11.9 years old) undergoing total knee arthroplasty (TKA) at Hartford Healthcare Bone & Joint Institute and transported them, submerged in PBS, to our lab within 8 h of extraction. A review by Institutional Review Board (IRB, Assurance #FWA00000601) found that this study does not constitute research involving human subjects according to 45 CFR 46.1 02(f) and therefore does not require further review or oversight by the IRB. After determining the local split-line directions (SLDs) by pricking the articular surfaces with a needle dipped in India ink, we extracted pairs of adjacent test specimens from locations across the joint cartilages. From each pair, we used one specimen for mechanical testing (cuboid, 3×3 mm^2 footprint, full thickness), with one through-thickness plane parallel to the local SLD, and the other for histological evaluation. We fixed the latter specimens immediately in 10% neutral buffered formalin, cf. Section 2.2. For the specimens undergoing mechanical testing, we carefully removed all of the underlying trabecular bone and as little subchondral bone as necessary to ensure the top (the articular surface) and bottom (the bone) surfaces were parallel.

We left the bone-cartilage interfaces intact to ensure boundary conditions at this interface mimicked *in situ* conditions.[28] We stored these specimens submerged in PBS at −80° prior to testing. On the day of a mechanical test, we thawed and glued (Super Glue Gel, Loctite) the articular surface and the subchondral bone (i.e., top and bottom) of a specimen to loading platens, ensuring a flat surface perpendicular to the stereo-camera system (front surface) and uncontaminated by glue [Fig. 1(a) and (b)]. We then air brushed (CM-C Plus, IWATA, Yokohama, JP) a speckle pattern on the front surface using a tissue marking dye (CDI's tissue Marking Dyes, Cancer Diagnostics, Durham, USA) diluted with deionized water (approximately 1:1). We let the speckle pattern air dry for 10 min, while keeping the other surfaces coated by PBS to prevent tissue dehydration and shrinking [Fig. 1(c) and (d)].

Histological assessments and quantification of constituents

To assess each specimen in terms of stage of degeneration, structural integrity, and tissue composition we follow the methodologies of Maier *et al.*.[29] We decalcified in 0.5 M EDTA, embedded specimens in paraffin, and sectioned them at 6 μm. We stained sections for each specimen with Safranin-O fast green (NovaUltra Safranin O stain kit, IHC World, Woodstock, USA) and Picosirius red (NovaUltra Sirius red stain kit, IHC World). We examined the latter under polarized light. Two trained observers analysed and interpreted images of the stained slides to obtain OARSI grades (FM, DMP)[5] and PLM-CO scores (FM, Lauren Marshall (LM)).[12] We considered only tissues up to OARSI grade 3.5 (moderate disease, presence of vertical fissures). For statistical analyses we binned specimens in three groups, based on OARSI grades: normal cartilage (grade < 2, group OA-1), mild OA ($2 \geq$ grade < 3, group OA-2), and moderate OA (grade ≥ 3, group OA-3); and based on their PLM-CO scores: normal collagen structure (score ≥ 4), mild disruption (score 3), and moderate disruption (score ≤ 2). To quantify the mass fractions of the constituents, we deparaffinized the embedded specimens, removed any subchondral bone, and measured their dry weights. We then rehydrated the specimens with a decreasing alcohol series to PBS,[30] measured their wet weights, and cut 10 mg pieces for analyses. We completed digestion and analyses using a Glycosaminoglycan (GAG) Assay Kit (6,022, Chondrex, Redmond, USA) and a Hydroxyproline Assay Kit (6,017, Chondrex). For GAG quantification we solubilized each specimen in 1.25 ml digestive solution (125 μg/ml Papain; 60,224, Chondrex) in PBS at pH 6.3 with 5 mM L-cystein-HCL and 10 mM EDTA-2Na, incubated at 65°C for 36 h. Subsequently, we hydrolyzed 100 μl of the dissolved tissue in 10 N hydrochloric acid to quantify the hydroxyproline concentration. We report all concentrations per wet weight.

Digital image correlation during applied shear strains

To apply prescribed shear strains, we used our testing device and protocol as previously described in Maier *et al.*.[27] We performed quasi-static (75 μm/min) cyclic simple shear tests and

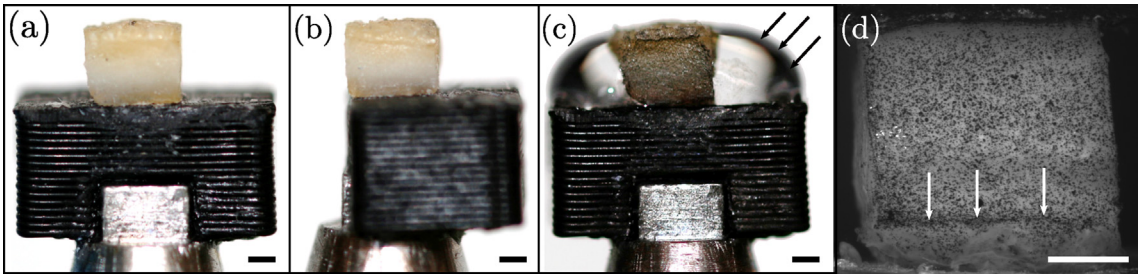

Fig. 1. Representative specimen glued to loading platen (black): (a) front, (b) side, and (c) back views. In (b) we see the flat surface perpendicular to the stereo-camera system. In (c) we see three sides of the specimen covered with phosphate buffered saline (PBS) (black arrows) while the speckle pattern dries. In (d) we see the final speckle pattern used for digital image correlation (DIC) recording, white arrows indicate the bone-cartilage interface. Scale bars equal 1 mm.

recorded images of the deformation in the SLD, i.e., with the front plane aligned with the SLD. We applied a 1% precompression and applied displacements corresponding to ±5, ±10 and ±15% shear strain. At each step in our protocol we allowed specimens to equilibrate, i.e., after gluing (2,000 s), after precompressing (4,000 s), and after increasing the strain magnitude (600 s). Our cyclic tests included three preconditioning cycles, and we recorded images of the fourth loading cycle to calculate patterns of displacement and strain. After completion of the full testing protocol, we applied tension to the specimen to verify the integrity of the glued interface. We completed all tests in a bath of PBS at 37°C (±1°C) including antibiotics (100 U/ml penicillin and 100 mg/ml streptomycin) and protease inhibitors (P2714, Sigma Aldrich, St. Louis, USA) to avoid tissue degeneration.

To record images for subsequent DIC, we used a stereo-camera system with two five-megapixel cameras (Manta G-505, Allied Vision, Stadtroda, DE). We adjusted the frame rate according to the applied displacement to record both loading and unloading in approximately 200–250 frames. To ensure accuracy of our measurements, we calibrated the camera setup before each test, and after allowing the bath of PBS to reach temperature.

Data analyses

We used the commercial software Istra4D (V4.4.3.414, Dantec Dynamics, Skovlunde, DK) for image processing and strain calculations. To track the deformation we established a grid pattern on the cartilage surface based on the speckle pattern. Our grid spacing of 10–15 pixels (depending on image quality) and pixel size of 3 μm resulted in a data point every 30–45 μm. We applied a local regression filter for the object contour based on an adaptive spline polynomial algorithm with a 5 × 5 kernel size. Applying Istra4D we approximated the displacement field by an analytic function (bicubic splines) to obtain 2-D deformation gradients for subsequent strain calculations. We used a grid-reduction factor of two (only direct-neighbor facets influence smoothing) and a smoothness factor of minus one (higher absolute value increases smoothing) for filtering (both recommended by manufacturer). We processed our image data through the full thickness of each specimen, from the articular surface to the subchondral bone. In our images the transition from cartilage to bone was clearly visible as a dark line (cf. Fig. 1(d)), and this served as a marker for the lower boundary. We exported the full field of 2-D Green–Lagrange tangential shear strain calculated as

$$E_{XY} = \frac{1}{2}\left(\frac{\partial u_X}{\partial Y} + \frac{\partial u_Y}{\partial X} + \frac{\partial u_X}{\partial X}\frac{\partial u_X}{\partial Y} + \frac{\partial u_Y}{\partial X}\frac{\partial u_Y}{\partial Y}\right) \quad (1)$$

We performed further processing and analyses using MATLAB (R2017b, The MathWorks, Natick, USA). First, we averaged (mean ± standard deviation) the shear strain values along horizontal lines at each height through the thickness of the specimen to generate a through-thickness strain curve. To avoid edge effects (cf. 18) we excluded approximately 10% of our data on each side of the front area (from the edges inwards). We then grouped those curves by either OARSI grade or PLM-CO score (Section 2.2) and averaged them to obtain master curves representing normal, mildly degenerated, and moderately degenerated cartilage. We also calculated the relative zonal recruitment R_i with $i \in \{\mathrm{DZ}, \mathrm{MZ}, \mathrm{SZ}\}$ as

$$R_{\mathrm{DZ}} = \frac{t_{\mathrm{DZ}} E_{XY,\mathrm{DZ}}}{E_{XY,\mathrm{blk}}},\ R_{\mathrm{MZ}} = \frac{t_{\mathrm{MZ}} E_{XY,\mathrm{MZ}}}{E_{XY,\mathrm{blk}}} \quad (2)$$

where t_i is the relative thickness of the corresponding zone, i.e., 0.3 for the DZ and 0.5 for the MZ,[31] and where $E_{XY,i}$ is the averaged Green–Lagrange shear strain in zone i. We calculated the bulk shear strain as $E_{XY,\mathrm{blk}} = \gamma_{\mathrm{app}}/2$, with $\gamma_{\mathrm{app}} = u_{X,\mathrm{max}}/t$, where $u_{X,\mathrm{max}}$ is the maximum applied displacement causing shearing and t is the thickness of the cartilage (top loading platen to the subchondral bone) measured from the DIC images. To account for data potentially missing near the articular surface (we considered up to 3% of the total thickness acceptable), we calculated the relative zonal recruitment of the SZ R_{SZ} as

$$R_{\mathrm{SZ}} = 1 - (R_{\mathrm{MZ}} + R_{\mathrm{DZ}}) \quad (3)$$

In this way the sum of the three zonal recruitments always equals 100% recruitment.

Statistical analyses

First we used a Shapiro–Wilk test to confirm that our data was normally distributed. To validate inter-observer agreement in our application of the OARSI and PLM-CO grading methods, we calculated the linear-weighted Cohen's kappa coefficient κ. We used an ANOVA analysis followed by a Tukey–Kramer post-hoc test to compare the relative zonal recruitment for each zone (SZ, MZ, and DZ) by OARSI and PLM-CO groups (Section 2.2). Finally, we used Pearson's correlation coefficient to determine the effect of age, specimen thickness, and content of collagen and GAG (number of comparisons $m = 4$) on the relative zonal recruitment. We used $\alpha = 0.05$ to test for significance and adjusted this with the Bonferroni-Holm method to account for multiple comparisons ($\alpha = 0.05/m$).

Results

We completed a total of 132 shear tests using 44 cartilage specimens. We successfully imaged the distribution of deformation at three applied strain levels (5, 10, 15%) on most of the 44 specimens. Seven of our specimens showed signs of mechanical failure

during testing (one at 10% and six at 15% applied strain), visible as an instant drop in the measured force response, and we excluded these data from subsequent analyses. We provide a detailed summary relating each imaged pattern of deformation (applied strain magnitude) to the patient number and OARSI grade in Table A2.

Through-thickness patterns of shear strain

We observed three general shapes for the curves of averaged through-thickness Green–Lagrange shear strains consistent over all applied strain magnitudes, as shown in Fig. 2.

In all specimens we found the highest shear strains (by magnitude) at or near the articular surface. Normal tissue (OA-1) also showed a distinct relative peak in shear strain near the transition from the MZ to the DZ, near or at the advancing cartilage–bone interface [Fig. 2(d)]. With advancing OA (mild degeneration, OA-2) the through-thickness shear strain became more homogeneous [Fig. 2(h)]. Finally, with further advancing OA (moderate degeneration, OA-3) the shear strain became more heterogeneous with most of the deformation focused near the articular surface (Fig. 2(l)).

When we averaged the shear-strain response of all specimens binned by OARSI grade we observed the same three general curves (Fig. 3); however, the standard-deviation of the mean of the averaged curves does not show a clear distinction between all curves in all segments.

When we plotted the relative zonal recruitment, binned by OARSI grades [Fig. 4(a)–(c)] and PLM scores [Fig. 4(d)–(f)], we observed only one consistently significant difference in zonal recruitment during the progression of OA: in the DZ.

When grouped by OARSI grade, at 10% applied shear strain zonal recruitment in the SZ significantly increased with progressing OA, and zonal recruitment in the MZ and DZ increased in mild vs moderate OA. When grouped by PLM score a consistent distinction in the zonal recruitment in the DZ became evident. Zonal recruitment in the DZ was significantly larger in groups with a healthy or near-healthy organization of collagen (PLM score ≥ 4), than in any other groups. There was no significant difference in zonal recruitment for the MZ or SZ across PLM-CO scores.

Histological assessments and quantification of constituents

Our OARSI grading resulted in $n_{OA-1} = 17$, $n_{OA-2} = 16$, and $n_{OA-3} = 11$ specimens per binned group. Inter-observer agreement for the unbinned OARSI grades was 0.925 and for the binned OARSI-graded groups was 1.0. Our PLM-CO scoring resulted in $n_{PLM-2} =$

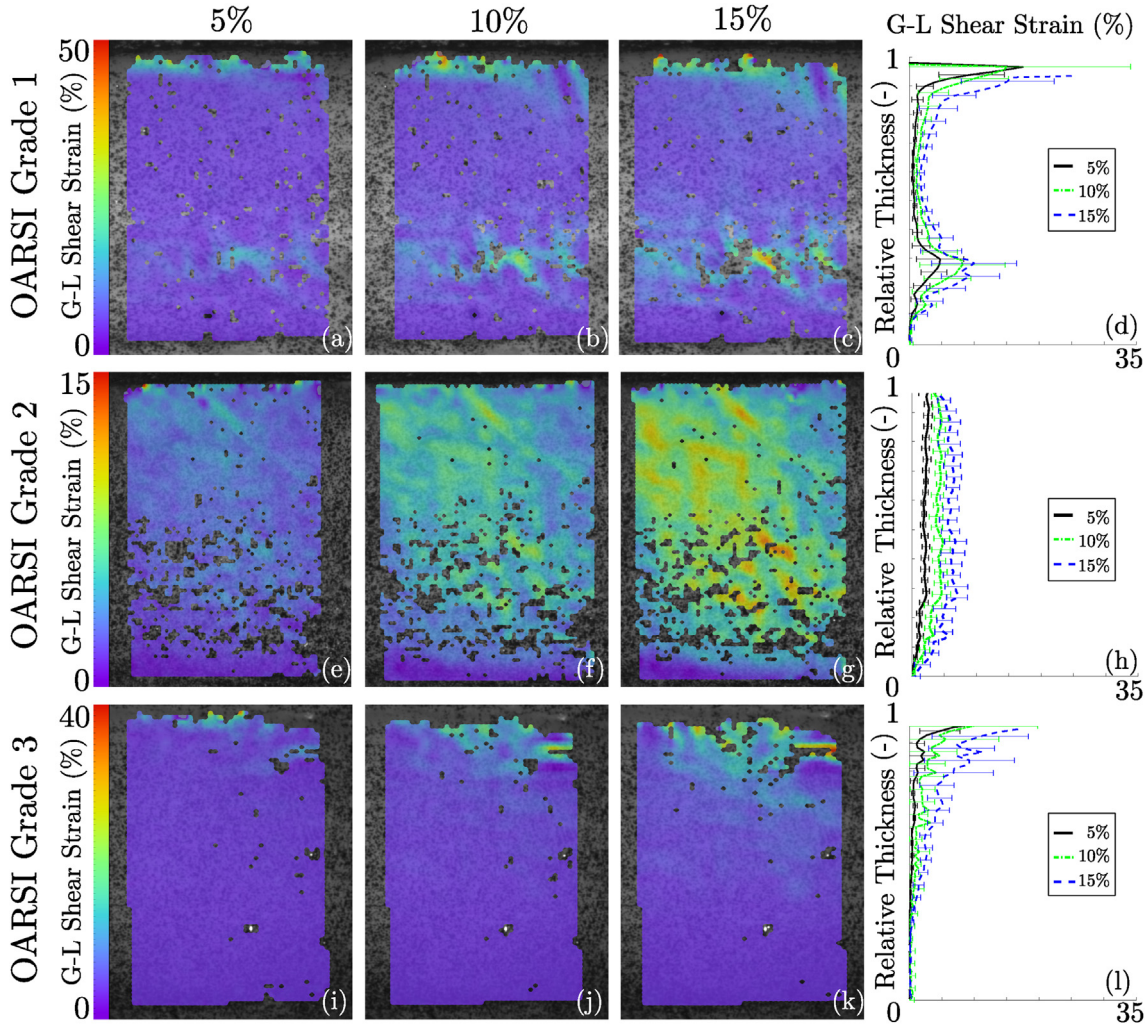

Fig. 2. Through-thickness patterns of shear strain evolve characteristically in early osteoarthritis. Representative through-thickness patterns of 2-D Green–Lagrange shear strain at applied bulk shear strains $\gamma = 5\%, 10\%, 15\%$ (columns 1, 2, 3) and corresponding averaged through-thickness shear strain response (column 4) with progressing osteoarthritis, i.e., increasing Osteoarthritis Research Society International (OARSI) grade 1, 2, 3 (rows 1, 2, 3).

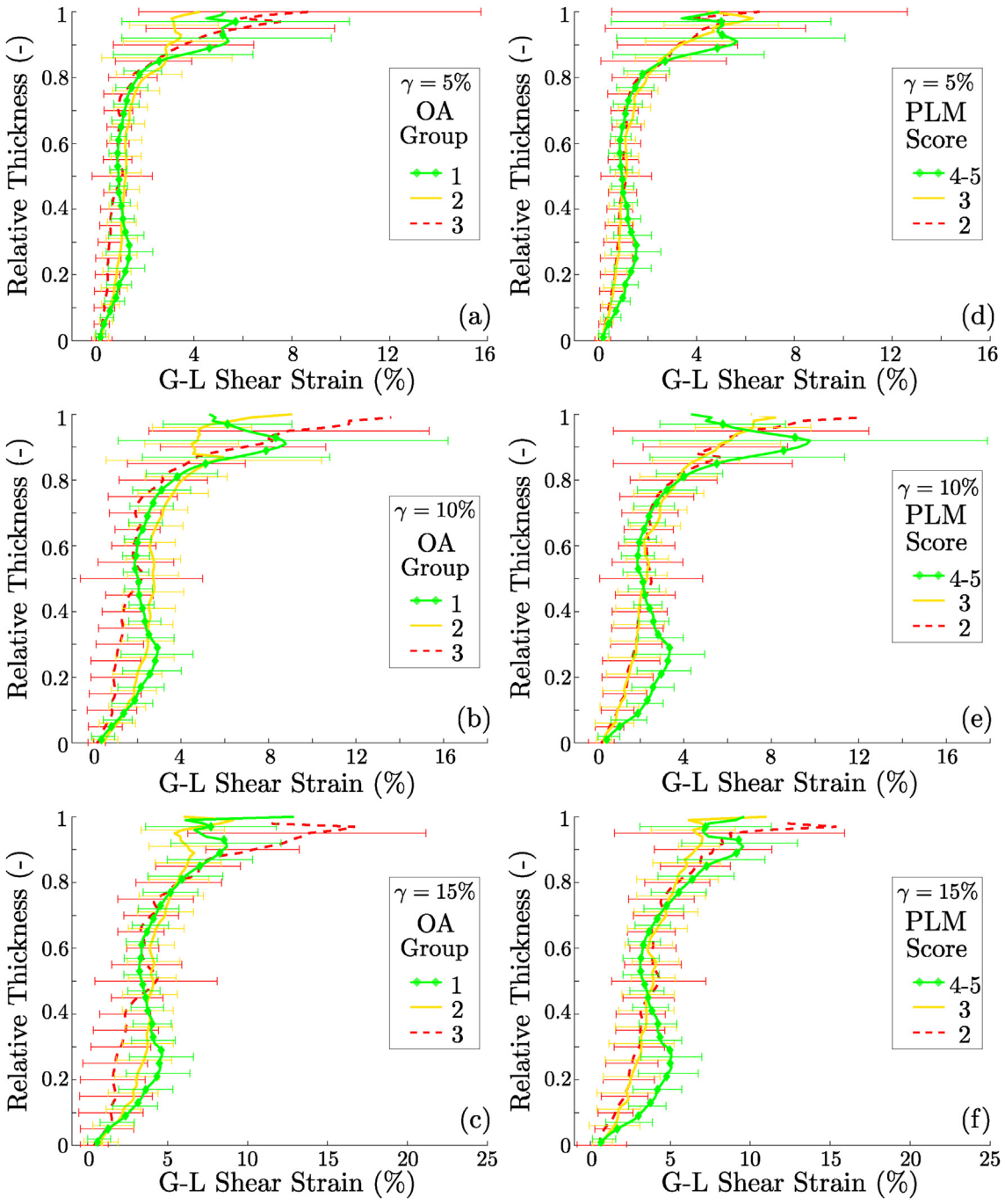

Fig. 3. Only specimens appearing normal in histology (OA-1) or specimens with normal zonal architecture (PLM–CO–4-5) present a distinct local peak in shear strain in the DZ. Through-thickness patterns of 2-D Green–Lagrange shear strain averaged by grouped OARSI grades (a–c) and PLM scores (d–f) at applied bulk shear strains $\gamma = 5\%, 10\%, 15\%$.

18, $n_{\mathrm{PLM-3}} = 12$, $n_{\mathrm{PLM-4}} = 10$, and $n_{\mathrm{PLM-5}} = 4$ specimens per binned group. For further statistical analyses we binned specimens with scores four and five into one group. Inter-observer agreement for the unbinned PLM score was 0.735 and for the binned PLM score 0.766.

We show specimen thicknesses, and measured GAG and total collagen concentration, grouped by both OARSI grades and PLM scores in Fig. 5.

Neither thickness nor either constituent showed a statistically significant change with increasing degeneration or loss of structural integrity.

Statistical analyses

We summarize the correlations of zonal recruitment with collagen content, age, and thickness in Table I.

Both bulk collagen content and age correlate significantly with increased zonal recruitment in the SZ and correspondingly reduced zonal recruitment in the DZ. Specimen thickness only correlates significantly at 15% applied strain, indicating reduced zonal recruitment in the DZ. We found no significant correlations among zonal recruitments and bulk GAG content. All correlations were relatively weak but significant.

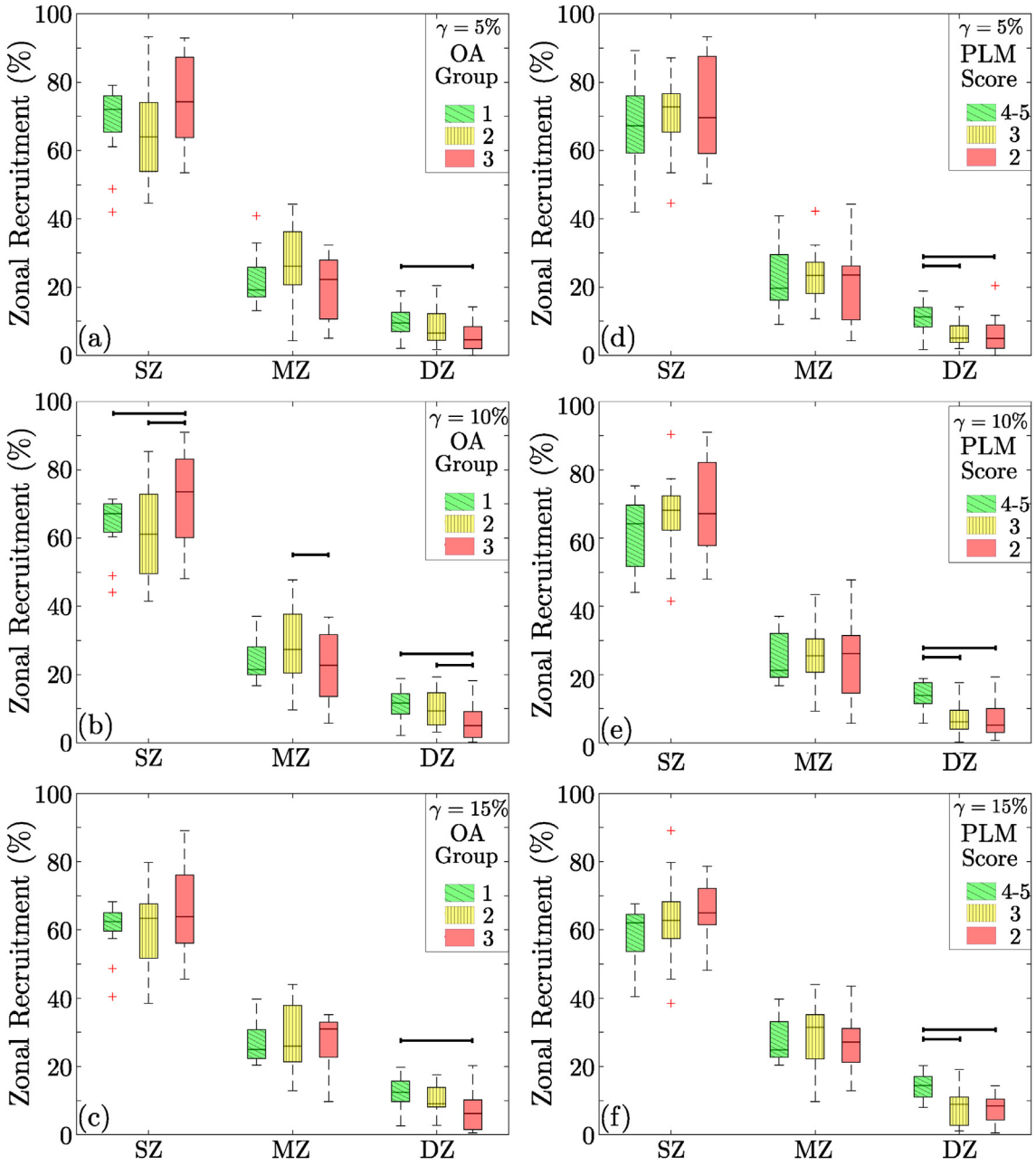

Fig. 4. Analyses of the zonal recruitment reveals that during the progression of early OA only the deep zone is recruited differently under shear in a statistically significant way. Relative zonal recruitment binned by grouped OARSI grades (a–c) and PLM scores (d–f) at applied bulk shear strains $\gamma = 5\%, 10\%, 15\%$. Black bars indicate significant differences ($p < 0.05$) between OARSI grades per zone.

Discussion

Through-thickness patterns of shear strain

We found three general qualitative through-thickness patterns of shear strain depending on the stage of degeneration of the specimens (cf. Fig. 3). Across all stages of degeneration (normal, mild, moderate) we found the highest strains, by magnitude and relative contribution, in the SZ. However, only a few specimens showed a distinct increase in shear strain in the transition between SZ and MZ, first reported by Buckley *et al.*[16] for healthy neonatal bovine tissue, and subsequently confirmed for human tissue.[32] Most of our specimens showed shear strain at the SZ comparable to Wong *et al.*.[18] They tested human articular cartilage in health and disease and found highest shear strains at the articular surface and without a distinct increase in shear strain in the transition between SZ and MZ.

We are the first to report a region of increased shear strains in normal cartilage in the transition from MZ to DZ, i.e., near the cartilage–bone interface (cf. Fig. 2(a)–(d)). Lai and Levenston[20] performed unconfined compression tests on cartilage explants and showed a similar increase in shear strain near the cartilage–bone interface. However, this was much smaller by magnitude than shear strains near the surface and thus they did not pursue it.

Our relative zonal recruitment provides information on the contribution of each through-thickness zone to the total

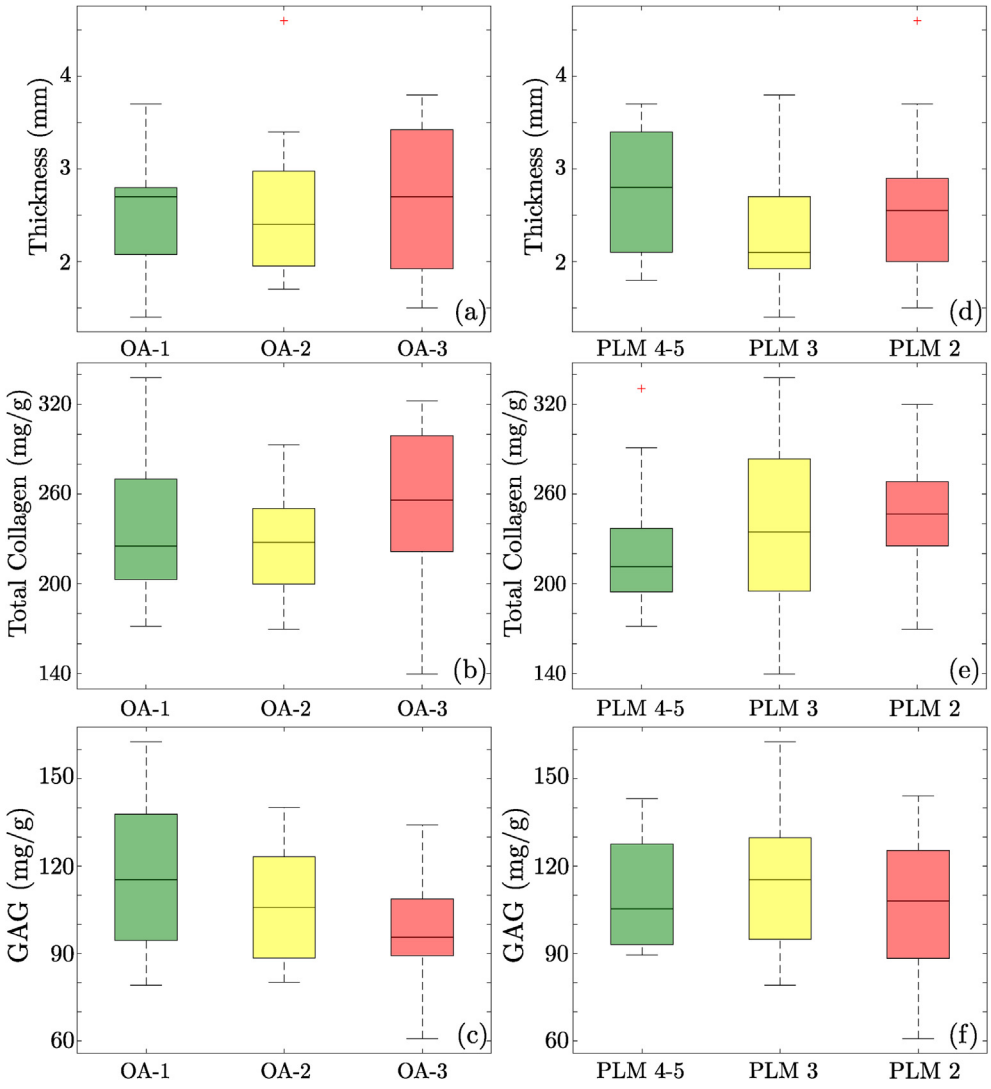

Fig. 5. Neither thickness nor the investigated constitutes vary significantly with OARSI grade or PLM score. Specimen thickness, GAG and total collagen content per wet weight by grouped OARSI grades (a–c) and PLM scores (d–f).

deformation of a specimen. Interestingly, the relative zonal recruitment of the DZ decreases with progressing OA (OARSI grade) and microstructural remodeling (PLM-CO score), while the MZ and SZ are not consistently (at all applied strain magnitudes) significantly affected. The DZ of all specimens appeared intact (PLM-CO >1) while we observed degeneration of the zones above, i.e., changes in the thickness ratios of SZ and MZ, as well as complete remodeling of the SZ. Thus, while OA likely initiates at the articular surface,[33] the patterns of shear strain in the DZ and, as a consequence, the mechanobiological environment of the chondrocytes within, are affected in the early stages of both OA (OARSI grade >2.5) and collagen-network remodeling (PLM-CO score ≤ 4). The mechanosensitivity of chondrocytes[34] suggests that the alteration in environment may stimulate changes in matrix synthesis, potentially initiating or accelerating a degenerative cascade. The formation and re-absorption of calcified cartilage also corresponds to changes in the biomechanical environment,[35,36] thus potentially favoring or initiating advancement of the calcification front, i.e., tidemark duplication, associated with OA[37] and often accompanied by collagen fibrillation at the articular surface.[38]

Assessing the zonal recruitments by PLM-CO score showed that strains in the DZ are higher when the zones above are intact, thus it appears that softening of the SZ and MZ, rather than stiffening of the DZ, causes the reduction in shear strain. However, improved imaging modalities capable of accurately imaging the tidemark, e.g.,37, and through-thickness indentation tests[39] could further clarify this point. The lack of correlation between our proposed zonal recruitment and GAG content indicates that structural or mechanical changes may precede other biochemical changes associated with early OA, consistent with Desrochers *et al.*.[9]

Our experiments have very little out-of-plane deformation (confirmed by our stereo-camera setup), and our applied speckle pattern is not heterogeneously compressed, both effects aiding the quality of our DIC. The quasi-static nature of our experiments does not represent deformation rates *in vivo*, where healthy cartilage can generate substantial interstitial fluid pressure. However, our experiments do allow us to measure patterns of deformation unaffected by inter-tissue fluid flow and to investigate local deformations of the solid constituents, thus identifying changes in the solid matrix that may be masked by alterations in bulk permeability.[40] We applied consistent bulk displacements (strains) to our specimens rather than bulk forces, to ensure comparable bulk deformations across different stages of OA. A multitude of changes to the mechanical properties accompany disease

Table I
Higher bulk collagen content leads to increased shear strains in the superficial zone (SZ) and corresponding reductions in the middle zone (MZ) and deep zone (DZ) under applied bulk shear strain. Pearson correlation coefficient *r* and corresponding level of significance *P* for correlation of relative zonal recruitment with collagen content, age, and thickness at applied bulk shear strains $\gamma = 5\%, 10\%, 15\%$. N.B. Only results with $P < 0.05$ shown. An asterisk indicates results considered significant after the Bonferroni-Holm adjustment

γ (%)	Zone		Collagen	Age	Thickness
5	SZ	*r*	0.4007	0.3396	–
		P	0.0085*	0.0278	–
	MZ	*r*	− 0.3816	–	–
		P	0.0127	–	–
	DZ	*r*	− 0.3120	− 0.5033	–
		P	0.0442	0.0007*	–
10	SZ	*r*	0.4977	0.3536	–
		P	0.0009*	0.0233	–
	MZ	*r*	− 0.4428	–	–
		P	0.0037*	–	–
	DZ	*r*	− 0.4204	− 0.6068	–
		P	0.0062*	< 0.0001*	–
15	SZ	*r*	0.5712	0.4804	− 0.3410
		P	0.0004*	0.0040*	0.0484
	MZ	*r*	− 0.5068	–	–
		P	0.0022*	–	–
	DZ	*r*	− 0.4297	− 0.7464	0.4897
		P	0.0112*	< 0.0001*	0.0033*

progression, e.g., reductions in stiffnesses[41] and alterations in time-dependent responses,[9] making it challenging to predict total deformations under applied forces and thus to stay within the field of view of our stereo stereo-camera system.

Histological assessments and quantification of constituents

Semi-quantitative, histology-based methods for assessing cartilage degeneration have inherent drawbacks: e.g., these discrete categories likely cannot fully capture the dynamic, years-long progression of disease in its full complexity. To estimate local degeneration we quantified the OARSI grade rather then the complete OARSI score.[5]

We attempted to utilize the histological images from slides stained with Picosirius red to extract specimen-specific zonal thicknesses for each specimen as a mask to calculate zonal recruitments. Unfortunately not all specimens showed three distinct through-thickness zones, despite the early stages of degeneration, highlighting the early occurrence of remodeling. Thus, we selected a generic mask (0.2/0.5/0.3 for SZ/MZ/DZ) based on Mow *et al.*[31] This idealized mask could serve in the future as a clinal diagnostic marker since the real *in vivo* zonal architecture is generally not obtainable.

The GAG and total collagen concentrations per wet weight that we measured are within ranges reported previously.[41,42,31] The lack of significant correlation with increasing degeneration (OARSI grades) and loss of structure (PLM scores) may indicate that these measures may not be sufficiently sensitive to identify early OA (OARSI grades 1–3).

Statistical analyses

Interestingly, bulk collagen content correlated with through-thickness patterns of shear strain, but it did not correlate with degeneration and loss of structure. Higher collagen content correlated with greater zonal recruitment in the SZ and a reduced contribution of the zones below it. This may indicate through-thickness patterns of strain can reveal subtle changes in the composition of cartilage, changes not clearly captured by histology. We further observed a shift in relative zonal recruitment from the DZ to the SZ with age; however, our data does not allow us to determine if this phenomenon is induced by age or disease. These correlations, while statistically significant, were relatively weak. We found no significant difference between specimens (binned by OARSI group), originating from different patients in support of our assumption to treat all specimens individually in our statistical analyses, consistent with our previous studies.[27,29]

Limitations and outlook

Large shear strains, applied as simple shears may not mimic the deformation *in vivo*, dominated by compressive loading. However, despite predominately external compression to cartilage *in vivo*, shear strains within the tissue tend to exceed compressive strains.[43] Additionally, with progression of OA the lubrication between contact surfaces decreases[44] and surface roughness also increases;[5] thus largely simple-shear deformations caused by higher friction may play an increasing role as OA progresses. We included only cartilage from the lateral femoral condyle while degeneration generally initiates at the medial chondyle.[45] Mechanical properties of lateral vs medial condyle appear indistinguishable,[46] so the increased incidence of OA seems to be a consequence of differences in loading rather than tissue mechanics.

In this study, specimens with a normal appearance still originate from knees affected by OA, so we do not have a fully healthy group as a control. Our normal group may still present compromised load-bearing capabilities despite near-healthy appearances 4,9. In OA the synovial fluid contains more matrix degrading proteins[47] and lubricates the cartilage interfaces less 44, thus affecting the entire joint. Furthermore, due to technical challenges we were not able to test a sufficient number of cartilage explants presenting severe signs of degeneration (OARSI grade > 4).

Our experiments revealed drastic alterations in the through-thickness distributions of shear strains at the very early stages of OA, as quantified by the OARSI grade. Specimens with a healthy appearance (OARSI Grade < 2) generally showed a band of shear strains in the DZ, which vanished with progressing OA and concurrent structural remodeling. With progression of OA the distribution of shear strains underneath the articular surface first became more homogeneous, followed by increasing heterogeneity, with a concentration of shear deformation in the SZ/MZ and no apparent deformation deeper within the tissue. Thus, OA affects the entirety of cartilage (through the thickness) even at very early stages, while OA is generally considered to initialize at the articular surface or the SZ.[48,49] Improved imaging techniques based on MRI have the potential for accurate, non-invasive assessment of cartilage health, particularly beyond the articular surface.[50,4] Among the various imaging protocols dualMRI provided the strongest correlations with OA severity.[13] However, insufficient resolution currently limits the measurement accuracy of distributions of strains *in-vivo*.[43] Our experiment provides sufficient resolution to identify a potential target for future studies incorporating improved MRI to verify whether the reduction in DZ recruitment and the qualitative change in shape of the through-thickness patterns of strains can serve as biomarkers sensitive to the onset of OA.

Author contributions

DMP oversaw the project; FM and DMP contributed to conception and design; CGL contributed tissues; FM prepared specimens and conducted the experiments; FM and DMP analyzed and interpreted data; FM and DMP participated in drafting the article; FM, CGL, and DMP revised the article critically; and FM, CGL, and DMP gave final approval of the version submitted.

Conflicts of interest statement
We have no conflicts of interest to report.

Role of the funding source
Any opinions, findings, and conclusions or recommendations expressed in this material are those of the author(s) and do not necessarily reflect the views of the National Science Foundation.

Acknowledgments

This material is based upon work supported by the National Science Foundation under Grant Number 1662429. We thank the orthopedic surgeons of Hartford Healthcare Bone & Joint Institute, Lauren Marshall (LM), and Victoria Blair.

Appendix A

We provide a detailed summary relating each mechanical test (applied strain magnitude) to the patient number and OARSI grade used for statistical analyses in Table A2.

Table A2
Detailed summary relating each mechanical test (applied strain magnitude) to the patient number and OARSI grade used for statistical analyses. A decreasing number of tests across one row indicates that specimen(s) failed mechanically. The total number of tests shown at the bottom is the number of data available for statistical analyses at each strain magnitude. M and F denote male and female, respectively.

Patient	Gender	OARSI	Specimens at applied strain γ (%)		
		Grade	5	10	15
1	F	1	3	3	3
		2	2	2	2
2	M	1	2	2	1
		2	2	2	1
		3	1	0	0
3	F	1	2	2	2
		2	2	2	2
4	M	1	1	1	1
		2	4	4	4
		3	1	1	0
5	F	1	1	1	1
		2	2	2	2
		3	2	2	2
6	F	1	2	2	2
7	F	1	3	3	3
		2	2	2	2
		3	1	1	1
8	F	2	4	4	3
		3	3	3	3
9	F	1	3	3	3
		2	1	1	1
Total Number *n*			44	43	39

References

1. Sandell LJ, Aigner T. Articular cartilage and changes in Arthritis: cell biology of osteoarthritis. Arthritis Res Ther 2001;3:107–13.
2. Loeser RF, Goldring SR, Scanzello CR, Goldring MB. Osteoarthritis: a disease of the joint as an organ. Arthritis Rheum 2012;64:1697–707.
3. Correa D, Lietman SA. Articular cartilage repair: current needs, methods and research directions. Semin Cell Dev Biol 2017;62:67–77.
4. Casula V, Hirvasniemi J, Lehenkari P, Ojala R, Haapea M, Saarakkala S, *et al.* Association between quantitative MRI and ICRS arthroscopic grading of articular cartilage. Knee Surg Sport Traumatol Arthrosc 2016;24:2046–54.
5. Pritzker KPH, Gay S, Jimenez SA, Ostergaard K, Pelletier JP, Revell PA, *et al.* Osteoarthritis cartilage histopathology: grading and staging. Osteoarthritis Cartilage 2006;14:13–29.
6. Mankin HJ, Dorfman H, Lippiello L, Zarins A. Biochemical and metabolic abnormalities in articular cartilage from osteoarthritic human hips. II Correlation of morphology with biochemical and metabolic data. J Bone Joint Surg Am 1971;53:523–37.
7. Outerbridge RE. The etiology of chondromalacia patellae. Bone Joint Lett J 1961;43-B:752–7.
8. Brittberg M, Winalski C. Evaluation of cartilage injuries and repair. J Bone Joint Surg Am 2003;85:58–69.
9. Desrochers J, Amrein MW, Matyas JR. Viscoelasticity of the articular cartilage surface in early osteoarthritis. Osteoarthritis Cartilage 2012;20:413–21.
10. Moger CJ, Barrett R, Bleuet P, Bradley DA, Ellis RE, Green EM, *et al.* Regional variations of collagen orientation in normal and diseased articular cartilage and subchondral bone determined using small angle X-ray scattering (SAXS). Osteoarthritis Cartilage 2007;15:682–7.
11. Goldring MB, Goldring SR. Articular cartilage and subchondral bone in the pathogenesis of osteoarthritis. Ann N Y Acad Sci 2010;1192:230–7.
12. Changoor A, Nelea M, Méthot S, Tran-Khanh N, Chevrier A, Restrepo A, *et al.* Structural characteristics of the collagen network in human normal, degraded and repair articular cartilages observed in polarized light and scanning electron microscopies. Osteoarthritis Cartilage 2011;19:1458–68.
13. Griebel AJ, Trippel SB, Emery NC, Neu CP. Noninvasive assessment of osteoarthritis severity in human explants by multicontrast MRI. Magn Reson Med 2014;71:807–14.
14. Soltz MA, Ateshian GA. Interstitial fluid pressurization during confined compression cyclical loading of articular cartilage. Ann Biomed Eng 2000;28:150–9.
15. Kurz B, Jin M, Patwari P, Cheng DM, Lark MW, Grodzinsky AJ. Biosynthetic response and mechanical properties of articular cartilage after injurious compression. J Orthop Res 2001;19:1140–6.
16. Buckley MR, Gleghorn JP, Bonassar LJ, Cohen I. Mapping the depth dependence of shear properties in articular cartilage. J Biomech 2008;41:2430–7.
17. Motavalli M, Whitney GA, Dennis JE, Mansour JM. Investigating a continuous shear strain function for depth-dependent properties of native and tissue engineering cartilage using pixel-size data. J Mech Behav Biomed Mater 2013;28:62–70.
18. Wong BL, Bae WC, Chun J, Gratz KR, Lotz M, Sah RL. Biomechanics of cartilage articulation: effects of lubrication and degeneration on shear deformation. Arthritis Rheum 2008;58:2065–74.
19. Gao LL, Qin XY, Zhang CQ, Gao H, Ge HY, Zhang XZ. Ratcheting behavior of articular cartilage under cyclic unconfined compression. Mater Sci Eng C 2015;57:371–7.
20. Lai JH, Levenston ME. Meniscus and cartilage exhibit distinct intra-tissue strain distributions under unconfined compression. Osteoarthritis Cartilage 2010;18:1291–9.
21. Hashimoto S, Nishiyama T, Hayashi S, Fujishiro T, Takebe K, Kanzaki N, *et al.* Role of p53 in human chondrocyte apoptosis in response to shear strain. Arthritis Rheum 2009;60:2340–9.
22. Silverberg JL, Barrett AR, Das M, Petersen PB, Bonassar LJ, Cohen I. Structure-function relations and rigidity percolation in the shear properties of articular cartilage. Biophys J 2014;107:1721–30.

23. Liu F, Kozanek M, Hosseini A, de Velde SKV, Gill TJ, Rubash HE, *et al*. *In vivo* tibiofemoral cartilage deformation during the stance phase of gait. J Biomech 2010;43:658–65.
24. Bingham JT, Papannagari R, Van de Velde SK, Gross C, Gill TJ, Felson DT, *et al*. In vivo cartilage contact deformation in the healthy human tibiofemoral joint. Rheumatology 2008;47:1622–7.
25. Mansour JM. Biomechanics of cartilage. In: Oatis C, Ed. Kinesiology: The Mechanics and Pathomechanics of Human Movement. Philadelphia, PA: Lippincott Williams and Wilkins; 2003:66–79.
26. Athanasiou KA, Darling EM, Hu JC. In: Articular Cartilage Tissue Engineering, vol. 1. San Rafael, CA: Morgan & Claypool Publishers; 2009.
27. Maier FS, Drissi H, Pierce DM. Shear deformations of human articular cartilage: certain mechanical anisotropies apparent at large but not small shear strains. J Mech Behav Biomed Mater 2017;65:53–65.
28. Morel V, Quinn TM. Cartilage injury by ramp compression near the gel diffusion rate. J Orthop Res 2004;22:145–51.
29. Maier F, Lewis CG, Pierce DM. The evolving large-strain shear responses of progressively osteoarthritic human cartilage. Osteoarthr Cartil 2019;27(5):810–22, https://doi.org/10.1016/j.joca.2018.12.025.
30. van Wijk XMR, Vallen MJ, van de Westerlo EM, Oosterhof A, Hao W, Versteeg EM, *et al*. Extraction and structural analysis of glycosaminoglycans from formalin-fixed, paraffin-embedded tissues. Glycobiology 2012;22:1666–72.
31. Mow VC, Gu WY, Chen FH. Structure and function of articular cartilage and meniscus. In: Mow VC, Huiskes R, Eds. Basic Orthopaedic Biomechanics & Mechano-Biology. 3rd edn. Philadelphia: Lippincott Williams & Wilkins; 2005:181–258.
32. Buckley MR, Bergou AJ, Fouchard J, Bonassar LJ, Cohen I. High-resolution spatial mapping of shear properties in cartilage. J Biomech 2010;43:796–800.
33. Hollander AP, Pidoux I, Reiner A, Rorabeck C, Bourne R, Poole AR. Damage to type II collagen in aging and osteoarthritis starts at the articular surface, originates around chondrocytes, and extends into the cartilage with progressive degeneration. J Clin Investig 1995;96:2859–69.
34. Grodzinsky AJ, Levenston ME, Jin M, Frank EH. Cartilage tissue remodeling in response to mechanical forces. Annu Rev Biomed Eng 2000;2:691–713.
35. O'Connor KM. Unweighting accelerates tidemark advancement in articular cartilage at the knee joint of rats. J Bone Miner Res 2009;12:580–9.
36. Schultz M, Molligan J, Schon L, Zhang Z. Pathology of the calcified zone of articular cartilage in post-traumatic osteoarthritis in rat knees. PLoS One 2015;10:1–12.
37. Mansfield JC, Winlove CP. A multi-modal multiphoton investigation of microstructure in the deep zone and calcified cartilage. J Anat 2012;220:405–16.
38. Revell PA, Pirie C, Amir G, Rashad S, Walker F. Metabolic activity in the calcified zone of cartilage: observations on tetracycline labelled articular cartilage in human osteoarthritic hips. Rheumatol Int 1990;10:143–7.
39. Hargrave-Thomas E, van Sloun F, Dickinson M, Broom N, Thambyah A. Multi-scalar mechanical testing of the calcified cartilage and subchondral bone comparing healthy vs early degenerative states. Osteoarthritis Cartilage 2015;23:1755–62.
40. Workman J, Thambyah A, Broom N. The influence of early degenerative changes on the vulnerability of articular cartilage to impact-induced injury. Clin Biomech 2017;43:40–9.
41. Franz T, Hasler EM, Hagg R, Weiler C, Jakob RP, Mainil-Varlet P. In situ compressive stiffness, biochemical composition, and structural integrity of articular cartilage of the human knee joint. Osteoarthritis Cartilage 2001;9:582–92.
42. Buckwalter JA, Mankin HJ, Grodzinsky AJ. Articular cartilage and osteoarthritis. Instr Course Lect 2005;54:465–80.
43. Chan DD, Cai L, Butz KD, Trippel SB, Nauman EA, Neu CP. *In vivo* articular cartilage deformation: noninvasive quantification of intratissue strain during joint contact in the human knee. Sci Rep 2016;6:19220.
44. Elsaid KA, Jay GD, Warman ML, Rhee DK, Chichester CO. Association of articular cartilage degradation and loss of boundary-lubricating ability of synovial fluid following injury and inflammatory arthritis. Arthritis Rheum 2005;52:1746–55.
45. Muehleman C, Bareither D, Huch K, Cole AA, Kuettner KE. Prevalence of degenerative morphological changes in the joints of the lower extremity. Osteoarthritis Cartilage 1997;5:23–37.
46. Deneweth JM, Arruda EM, McLean SG. Hyperelastic modeling of location-dependent human distal femoral cartilage mechanics. Int J Non-Linear Mech 2015;68:146–56.
47. Roach HI, Yamada N, Cheung KSC, Tilley S, Clarke NMP, Oreffo ROC, *et al*. Association between the abnormal expression of matrix-degrading enzymes by human osteoarthritic chondrocytes and demethylation of specific CpG sites in the promoter regions. Arthritis Rheum 2005;52:3110–24.
48. Panula HE, Hyttinen MM, Arokoski JPA, Långsjö TK, Pelttari A, Kiviranta I, *et al*. Articular cartilage superficial zone collagen birefringence reduced and cartilage thickness increased before surface fibrillation in experimental osteoarthritis. Ann Rheum Dis 1998;57:237–45.
49. Pearle AD, Warren RF, Rodeo SA. Basic science of articular cartilage and osteoarthritis. Clin Sports Med 2005;24:1–12.
50. MacKay JW, Low SBL, Smith TO, Toms AP, McCaskie AW, Gilbert FJ. Systematic review and meta-analysis of the reliability and discriminative validity of cartilage compositional MRI in knee osteoarthritis. Osteoarthritis Cartilage 2018;26:1140–52.